Biochemical and Functional Evaluation of the Intramolecular Disulfide Bonds in the Zinc-Chelating Antimicrobial Protein Human S100A7 (Psoriasin)

Citation: Cunden, Lisa S. et al. "Biochemical and Functional Evaluation of the Intramolecular Disulfide Bonds in the Zinc-Chelating Antimicrobial Protein Human S100A7 (Psoriasin)." Biochemistry 56, 43 (October 2017): 5726-5738 © 2017 American Chemical Society

As Published: http://dx.doi.org/10.1021/acs.biochem.7b00781

Publisher: American Chemical Society (ACS)

Persistent URL: https://hdl.handle.net/1721.1/123654

Version: Author's final manuscript: final author's manuscript post peer review, without publisher's formatting or copy editing

HHS Public Access

Author manuscript

Biochemistry. Author manuscript; available in PMC 2018 October 31.

Published in final edited form as:

Biochemistry. 2017 October 31; 56(43): 5726–5738. doi:10.1021/acs.biochem.7b00781.

Biochemical and Functional Evaluation of the Intramolecular Disulfide Bonds in the Zinc-Chelating Antimicrobial Protein Human S100A7 (Psoriasin)

Lisa S. Cunden[1], **Megan Brunjes Brophy**[1], **Grayson E. Rodriguez**[1], **Hope A. Flaxman**[1], and **Elizabeth M. Nolan**[1,*]

[1]Department of Chemistry, Massachusetts Institute of Technology, Cambridge, MA 02139, United States

Abstract

Human S100A7 (psoriasin) is a metal-chelating protein expressed by epithelial cells. It is a 22-kDa homodimer with two EF-hand domains per subunit, and two transition-metal-binding His_3Asp sites at the dimer interface. Each subunit contains two cysteine residues that can exist as free thiols ($S100A7_{red}$) or as an intramolecular disulfide bond ($S100A7_{ox}$). Herein, we examine the disulfide bond redox behavior, the Zn(II) binding properties, and the antibacterial activity of S100A7, as well as the effect of Ca(II) ions on these properties. In agreement with prior work, (Hein *et al. Proc. Natl. Acad. Sci. U. S. A.* **2013**, *112,* 13039–13044), we show that apo $S100A7_{ox}$ is a substrate for the mammalian thioredoxin system; however, negligible reduction of the disulfide bond is observed for Ca(II)- and Zn(II)-bound $S100A7_{ox}$. Furthermore, metal binding depresses the midpoint potential of the disulfide bond. $S100A7_{ox}$ and $S100A7_{red}$ each coordinate two equivalents of Zn(II) with sub-nanomolar affinity in the absence and presence of Ca(II) ions, and the cysteine thiolates in $S100A7_{red}$ do not form a third high-affinity Zn(II) site. These results refute a prior model implicating the Cys thiolates of $S100A7_{red}$ in high-affinity Zn(II) binding (Hein *et al. Proc. Natl. Acad. Sci. U. S. A.* **2013**, *112,* 13039–13044). $S100A7_{ox}$ and the disulfide-null variants show comparable Zn(II)-depletion profiles; however, only $S100A7_{ox}$ exhibits antibacterial activity against several bacterial species. Metal substitution experiments suggest that the disulfide bonds in S100A7 may enhance metal sequestration by the His_3Asp sites and thereby confer growth inhibitory properties to $S100A7_{ox}$.

Graphical Abstract

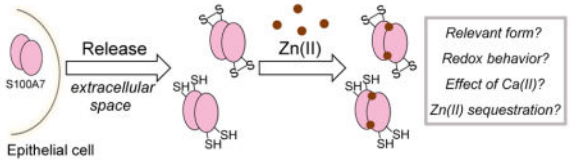

*Corresponding author: lnolan@mit.edu, Phone: 617-452-2495.

Supporting Information

Complete Experimental Methods, design of the S100A7 variant synthetic genes, Tables S1–S4, Figures S1–S24, and supporting references. This material is available free of charge via the Internet at http://pubs.acs.org.

Epithelial surfaces are continuously exposed to a variety of microbial challenges and thus maintain a complex biochemical barrier that prevents infections and preserves the ensemble of microbes that constitute the normal microflora.[1] The production and release of multiple innate immune factors is one strategy employed by epithelial cells for barrier protection.[2,3] Human S100A7 (psoriasin, Figure 1) is a Ca(II)- and Zn(II)- chelating host-defense protein that is expressed by epithelial cells and secreted into the upper layers of the epithelium.[4–7] It contributes to the innate immune response as well as cell differentiation, epidermal maturation, and epithelial tumorigenesis.[6,8,9] S100A7 is recognized as an antimicrobial factor of the skin as well as the human tongue, esophagus and female genital tract.[10–13] Several mechanisms for the antimicrobial activity of S100A7 have been proposed.[10,12,1415] Seminal studies reported that S100A7 has antibacterial activity against *Escherichia coli*, a microbe that rarely colonizes the skin and oral cavity.[10] Later work revealed that $S100A7_{red}$ and $S100A7_{ox}$ have antifungal activity against filamentous fungi, including the dermatophyte *Trichophyton rubrum* and *Aspergillus fumigatus*.[12] These two investigations pointed to a role of the Zn(II)-binding sites of S100A7 in antimicrobial function,[10,12] and thus indicated a putative contribution to nutritional immunity, an innate immune response that limits nutrient metal availability to microbes.[16,17] Furthermore, human S100A7 damages the cell membrane of *Bacillus megaterium*, suggesting an alternative model for its antimicrobial activity by membrane permeabilization.[15] Along these lines, a putative frog orthologue of S100A7, which lacks the Zn(II)-binding sites of human S100A7, was also shown to damage the cell membranes of *B. megaterium* and *Bacillus subtilis*.[18] A third model for S100A7 in host-defense focuses on its ability to adhere to *E. coli* and keratinocytes, and the occurrence of cross-linked S100A7 species in human wounds.[14] This model proposes that S100A7 functions as a solid-phase component of the physical barrier that protects the epithelium from microbial invasion, as well as a soluble antimicrobial protein in wound fluids.[14] Taken together, these studies suggest that the host-defense function S100A7 may be multi-faceted: the protein may exhibit different antimicrobial activity depending on the environmental milieu and microbe. Herein, we focus on the Zn(II)-chelating ability of human S100A7 and its putative contributions to the metal-withholding innate immune response.

Human S100A7 is a 22-kDa homodimer and member of the S100 family of Ca(II)-binding proteins (Figure 1). Each S100A7 subunit (101-aa, 11-kDa) contains two EF-hand domains (Figure 1D). The C-terminal EF-hand is “canonical” or calmodulin-like and binds Ca(II) in a 7-coordinate geometry.[6] The “non-canonical” N-terminal EF-hand domain provides a lower coordination number and is a hallmark of S100 polypeptides.[19] The N-terminal EF-hand of S100A7 is particularly noteworthy because its loop region is three residues shorter relative to those of other S100 polypeptides (e.g. S100A8, S100A9, S100A12), and it contains a Ser residue at position 30 (Figure 1D). This residue aligns with a Glu/Asp residue in the other S100 polypeptides, a bidentate ligand that binds Ca(II) at the N-terminal EF-hand.[6,20] In addition to the Ca(II) sites, the S100A7 homodimer harbors two His_3Asp motifs at the dimer interface. His87 and His91 of one monomer together with His18 and Asp25 of the second monomer form each His_3Asp site. Amino acid sequence alignment shows that these residues align with the metal-coordinating moieties of other human S100 polypeptides, including S100A12 and the calprotectin subunits S100A8 and S100A9 (Figure 1D).

Crystal structures of Ca(II)-bound and Ca(II)- and Zn(II)-bound S100A7 provide snapshots of the Ca(II)- and Zn(II)-binding sites (Figure 1A–C).[6] These two structures were obtained using ≥20 equivalents of Ca(II) in the crystallization conditions, and the C-terminal EF-hands contain bound Ca(II) whereas the N-terminal EF-hands do not.[6] The Ca(II)- and Zn(II)-bound S100A7 structure reveals a 2:1 Zn(II):S100A7 homodimer stoichiometry with a Zn(II) ion coordinated at each His_3Asp site in a distorted tetrahedral geometry (Figure 1B, 1C).

Another striking structural feature of S100A7 is the presence of Cys47 and Cys96, two cysteine residues that can form an intramolecular disulfide bond in each subunit of the homodimer (Figure 1C).[6,20] Amino acid sequence comparisons show that the ability to form an intramolecular disulfide in each subunit differentiates S100A7 from S100A8, S100A9, and S100A12 (Figure 1D). Intra- and intermolecular disulfide bond formation occurs for bovine S100B, a dimeric S100 protein abundant in the brain that exhibits two Cys residues per S100 subunit.[21–24] Notably, the Cys47–Cys96 disulfide bond of $S100A7_{ox}$ is in close proximity to the Zn(II)-binding site (Figure 1C). Indeed, Cys96 is separated from the Zn(II)-coordinating residue His91 by a Gly–Ala–Ala–Pro loop.

These observations highlight some fundamental questions pertaining to the disulfide bond redox chemistry, structure, and function of S100A7. In particular, do $S100A7_{red}$ and $S100A7_{ox}$ exhibit different biophysical and functional properties? Are both the oxidized and reduced forms physiologically significant? A recent analysis of extracts from lesional psoriasis scales identified $S100A7_{red}$ as an antifungal component of this mixture, indicating that the reduced form can exist *in vivo*.[12] This discovery motivated evaluation of the antimicrobial activity of $S100A7_{ox}$, $S100A7_{red}$ and the disulfide-null variant S100A7-Ala, and resulted in a new proposal that the redox states of the Cys residues in S100A7 modulate its functional properties.[12]

In this work, we address outstanding questions pertaining to the disulfide bond redox chemistry, Zn(II)-binding properties, and antibacterial activity of human S100A7. Because S100A7 is a Ca(II)-binding protein that is secreted from the cytoplasm, where Ca(II) levels are low (i.e. nanomolar), to the extracellular space where Ca(II) levels are high (i.e. ≈2 mM),[2526] we also consider the effects of Ca(II) ions on the behavior of this protein. To evaluate $S100A7_{ox}$ and $S100A7_{red}$, we describe methods to prepare these two forms in high yield and purity following recombinant protein expression in *E. coli*. Because reported solution studies describing the Zn(II)-binding properties of S100A7 are, to the best of our knowledge, limited to one equilibrium dialysis experiment,[8] we probe its Zn(II)-binding stoichiometry and affinity, and investigate whether disulfide bond formation and Ca(II) ions affect Zn(II) binding. Towards deciphering the antibacterial activity of S100A7, we examine the metal-depletion profiles and growth inhibitory activity of $S100A7_{ox}$ and the disulfide-null variants S100A7-Ser and S100A7-Ala. We also employ Co(II)/Zn(II) substitution experiments to examine metal exchange at the His_3Asp sites. Taken together, our data provide fundamental insights into the disulfide bond redox behavior and coordination chemistry of S100A7, and suggest that the disulfide bond may enhance Zn(II) sequestration by the His_3Asp sites.

Materials and Methods

Full experimental details are provided as Supporting Information.

Results and Discussion

Preparation of S100A7 and Variants

We previously reported a procedure for obtaining apo human S100A7 in high yield following recombinant expression in *E. coli* BL21(DE3), column chromatography, and dialysis.[27] This procedure afforded S100A7 in high purity based on SDS-PAGE. Nevertheless, analytical HPLC revealed that this purification resulted in mixtures of $S100A7_{red}$ and $S100A7_{ox}$, with the reduced species being predominant. Thus, for the current work, we established protocols that provide homogenous samples of $S100A7_{red}$ and $S100A7_{ox}$. We also employed these general methods to obtain samples of $S100A7\Delta_{red}$ and $S100A7\Delta_{ox}$, variants that lack the His_3Asp metal-binding sites because the four amino acids comprising the His_3Asp site (His18, Asp25, His87, and His91) site were replaced by non-coordinating Ala residues (Table S1). These proteins serve as non-Zn(II)-binding controls.

We considered several approaches to obtain homogenous $S100A7_{ox}$. Starting from the $S100A7_{red}$/$S100A7_{ox}$ mixture obtained from the original purification protocol, attempts to fully oxidize the protein on a preparative scale by air oxidation or by using redox buffers containing glutathione- or cysteine-based redox systems proved unsuccessful. In all instances, mixtures of $S100A7_{red}$ and $S100A7_{ox}$ were obtained. We subsequently evaluated a procedure involving Cu(II)-catalyzed oxidation of thiols to disulfides, which proved to be successful. Although an uncommon method in protein purification, the Cu(II)-catalyzed oxidation of thiols to form intra- and intermolecular disulfides in proteins has been reported for bovine oxyhemoglobin,[28,29] human S100A8,[30] and bovine S100B.[23] Initial analytical-scale trials revealed that addition of Cu(II) to S100A7 under aerobic conditions resulted in nearly quantitative conversion to $S100A7_{ox}$. Optimization of the procedure yielded homogenous $S100A7_{ox}$ with negligible Cu contamination.

For the Cu(II)-catalyzed oxidation, we first purified S100A7 as previously described[27] except that we employed a Tris buffer (20 mM Tris, 100 mM NaCl, pH 7.5) in the final column purification by SEC. We selected a Tris buffer because precipitation occurred when the Cu(II)-catalyzed oxidation was carried out in the HEPES buffer that we routinely employ during S100 protein purification (75 mM HEPES, 100 mM NaCl, pH 7.0).[27, 31] We found that ≈100% conversion to $S100A7_{ox}$ could be achieved by incubating the protein with three equivalents of Cu(II) for 2 h at room temperature (Figure 2). Excess Cu(II) was employed in order to fully oxidize S100A7 because the two His_3Asp sites of S100A7 bind Cu(II). Following disulfide bond formation, the Cu was removed by extensive dialysis. ICP-MS of the resulting protein revealed ≈0.03 and ≈0.04 equivalents of contaminating Cu and Zn, respectively, per $S100A7_{ox}$ homodimer.

We obtained $S100A7\Delta_{ox}$ using the same procedure except that (i) two equivalents of Cu(II) were employed and (ii) a precipitate was removed by centrifugation after the 2-h incubation at room temperature, and the resulting soluble fraction was stirred overnight at room

temperature, which yielded the completely oxidized protein (Figure S1, Supporting Information).

We obtained homogenous $S100A7_{red}$ and $S100A7\Delta_{red}$ by simply dialyzing the S100A7 protein obtained from our reported procedure against Chelex resin in the presence of 1 mM DTT. We also prepared two disulfide-null variants, S100A7-Ser (S100A7(C47S)(C96S)) and S100A7-Ala (S100A7(C47A)(C96A)) using the original purification procedure.[27] These two variants serve as models for $S100A7_{red}$ because they allow for studies to be performed under aerobic conditions in the absence of reducing agents. In addition, comparisons of $S100A7_{red}$ to variants with Cys→Ser/Ala substitutions allow monitoring for potential functions of the free thiolates in the native protein.

We obtained the S100A7 proteins in yields that ranged from 30–80 mg/L of culture. Each protein was characterized by SDS-PAGE, analytical HPLC, ESI-MS, thiol quantification, CD spectroscopy, analytical SEC, and ICP-MS (Tables 1, S2, S3; Figures S2–S5). SDS-PAGE and analytical HPLC analysis revealed that all proteins were obtained in high purity (Figures S2, S3), ESI-MS afforded the expected mass for each protein, and free thiol quantification using DTDP further verified the redox states of $S100A7_{red}$ (≈4 free thiols per homodimer) and $S100A7_{ox}$ (≈0 free thiol per homodimer) (Table 1). The CD spectra showed local minima at 208 and 220 nm, confirming the expected α-helical secondary structure (Figure S4). Analytical SEC demonstrated that each apo protein was isolated as a homodimer, and that each protein eluted as a homodimer in the presence of excess Ca(II) and Zn(II), indicating that metal binding does not cause a change in quaternary structure (Figure S5). ICP-MS demonstrated low contaminating metal content in the purified proteins (Table S2).

The Thioredoxin System Reduces Apo $S100A7_{ox}$

In agreement with prior work,[12] we observed that apo $S100A7_{ox}$ is a substrate for the mammalian thioredoxin system. Analytical HPLC of samples from enzymatic activity assays conducted at pH 7.0 containing apo $S100A7_{ox}$, human Trx, rat liver TrxR, and NADPH revealed loss of $S100A7_{ox}$ (16.4 min, ±Met1) and formation of $S100A7_{red}$ (18.4 min, ±Met1) (Figure 3A). At the final 2-h time point, the reaction mixture predominantly contained $S100A7_{red}$. As expected, HPLC traces for the no-enzyme control showed no $S100A7_{red}$ formation over this time period (Figures 3B). This assay was performed aerobically, and it is possible that some background air oxidation of $S100A7_{red}$ occurred over the 2-h time course, which would regenerate the substrate (Figure S7). Next, we examined the effect of Ca(II) on the Trx/TrxR-catalyzed reduction of the Cys47–Cys96 disulfide bond in $S100A7_{ox}$. When we included 2 mM Ca(II) in the assay buffer, we observed less formation of $S100A7_{red}$; integration of the peak areas revealed that the S100A7 mixtures contained only ≈12% and ≈22% $S100A7_{red}$ at 15 and 120 min, respectively (Figure 3C). Prior investigations demonstrated that Ca(II) does not affect the enzymatic activity of Trx/TrxR.[32] In agreement, we performed Trx/TrxR activity assays using $HD5_{ox}$, a peptide with three disulfide bonds that does not coordinate Ca(II), as a substrate and observed comparable disulfide bond reduction in the absence and presence of 2 mM Ca(II) (Figure S8). When we pre-incubated $S100A7_{ox}$ with 1.9 equivalents of Zn(II)

to form the Zn(II):S100A7$_{ox}$ complex, negligible formation of S100A7$_{red}$ in the absence or presence of Ca(II) occurred (Figures 3D and 3E). Because Zn(II) is an inhibitor of the thioredoxin system,[32] we designed a control assay to probe whether the Zn(II) included in this assay poisoned the enzyme. Using the same assay conditions, we spiked the reaction mixture with HD5$_{ox}$, a Trx/TrxR substrate that does not bind Zn(II). We observed comparable reduction of HD5$_{ox}$ to HD5$_{red}$ in the absence and presence of Zn(II)-S100A7$_{ox}$, indicating that the Zn(II) was bound to S100A7$_{ox}$ and therefore did not inhibit the thioredoxin system (Figure S9). Thus, Zn(II) binding to S100A7$_{ox}$ prevents intramolecular disulfide bond reduction by Trx/TrxR. Taken together, these data suggest that Ca(II) and Zn(II) depress the redox potential of the intramolecular disulfide bonds in S100A7$_{ox}$. An alternative scenario is that metal binding causes a change in protein structure or dynamics that precludes enzymatic access to the disulfide bonds. However, apo, Ca(II)- bound, Zn(II)-bound, and Ca(II)- and Zn(II)-bound S100A7$_{ox}$ are homodimers and the Cys47–Cys96 disulfide bond is surface exposed in the crystal structures of S100A7 (Figure 1), making us favor the former possibility.

Ca(II) Ions Depress the Midpoint Potential of S100A7

In order to gain further insight into the redox behavior of S100A7, we determined the midpoint potential (E_m) of S100A7 at pH 7.0 in the absence and presence of 2 mM Ca(II) (Figure 4). We incubated anaerobic solutions of S100A7$_{ox}$ in glutathione-based buffers with defined redox potentials spanning the −400 to −200 mV range for 96 h at 37 °C. To demonstrate that redox equilibrium was reached, we verified that the protein speciation was unchanged at 96 h compared to earlier and later time points (Figure S10). Analytical HPLC of the equilibrium mixtures revealed varying ratios of peaks corresponding to S100A7$_{ox}$ and S100A7$_{red}$, and an S100A7-glutathione adduct was also identified (Figure S11). The E_m value of the S100A7 disulfide bond was determined from the equilibrium between S100A7$_{ox}$ and S100A7$_{red}$ as quantified by HPLC. It was first estimated by identifying the E_m value that provided a 1:1 ratio of S100A7$_{ox}$ and S100A7$_{red}$ (Figure 4). This simple analysis yielded values of ca. −255 (−Ca) and −298 (+Ca) mV. Subsequent data fitting showed that the data were not well fit using the Nernst equation (Figure S12). This poor data fitting occurred because all samples contained mixtures of S100A7$_{ox}$ and S100A7$_{red}$ at equilibrium. The percentage of S100A7$_{ox}$ in solution maximized at −200 mV where the mixtures contain ≈93 and ≈96% S1007$_{ox}$ for apo and Ca(II)-bound S100A7, respectively (Figure 4). We therefore employed a logistic function and allowed the calculated maxima to vary during data fitting. In agreement with the simple by-the-eye analysis, this analysis provided E_m values of −255 (−Ca) and −298 (+Ca) mV (Figure S12). These values fall within the range expected for disulfide-containing peptides and proteins.[29,33–35] This work also provides a foundation for future experiment that address how additional experimental conditions of physiological relevance, such as changes in ionic strength, affect the redox properties of S100A7.

Further investigations are required to elucidate the molecular basis for how Ca(II) coordination depresses the E_m value of S100A7 by ≈50 mV. Overlaying the Ca(II)-free[20] and Ca(II)-bound[6] crystal structures suggests that Ca(II) binding by S100A7 does not cause a significant structural re-arrangement. However, in solution, Ca(II)-binding at the EF-hand

domains — and specifically the C-terminal EF hand, which is in closest proximity to the disulfide bridge (Figure 1D) — may affect protein dynamics such that intramolecular disulfide bond formation is favored. Ca(II) binding may decrease entropy and cause the regions around Cys47 and Cys96 to become more rigid, and prearrange these residues for disulfide bond formation.

We attempted to determine the midpoint potentials of Zn(II)- and Ca(II)- and Zn(II)-bound S100A7. These experiments were unsuccessful because we were unable to reduce Zn(II)-bound $S100A7_{ox}$, even under the most reducing conditions provided by the glutathione redox buffer system (−400 mV). We also observed that reduction of the disulfide bond in Zn(II)-bound $S100A7_{ox}$ by addition of excess GSH, DTT or TCEP occurs less readily than for its apo counterpart (Figure S13). Similar to the effect of Ca(II) ions on the E_m value of S100A7, Zn(II) coordination at the His_3Asp sites may stabilize or favor formation of the disulfide bridge.

Both $S100A7_{ox}$ and $S100A7_{red}$ Have Two High-Affinity Zn(II)-binding Sites

The crystal structure of Ca(II)- and Zn(II)-bound $S100A7_{ox}$ shows a Zn(II):$S100A7_{ox}$ homodimer stoichiometry of 2:1,[6] which is expected because of the two His_3Asp sites per homodimer. Nevertheless, the Zn(II)-binding stoichiometry of $S100A7_{red}$ has not been ascertained, and it was recently hypothesized that the free thiolates of Cys47 and Cys96 create a third high-affinity Zn(II) site in $S100A7_{red}$.[12] This notion originated from studies in which $S100A7_{red}$ exhibited greater antimicrobial activity than $S100A7_{ox}$ against the fungal pathogen *A. fumigatus*, which was attributed to more effective Zn(II)- sequestering activity by the reduced form.[12] To investigate the Zn(II)-binding stoichiometry of $S100A7_{ox}$ and $S100A7_{red}$ in solution, we performed Zn(II) competition experiments with each protein and the colorimetric Zn(II) indicator Zincon ($K_{d,Zn} \approx 10$ μM).[36,37] These titrations revealed that $S100A7_{ox}$ and $S100A7_{red}$ outcompete Zincon for two equivalents of Zn(II) in both the absence and presence of 2 mM Ca(II) (Figures 5 and S14), and that the free Cys residues in $S100A7_{red}$ do not form a third high-affinity Zn(II) site.

Both $S100A7_{ox}$ and $S100A7_{red}$ Bind Zn(II) with Sub-Nanomolar Affinity

To further probe the Zn(II) affinity of S100A7, we performed additional competition titrations with $S100A7_{ox}$, $S100A7_{red}$, and the variants S100A7-Ser, S100A7-Ala, and $S100A7\Delta_{ox}$. We examined the competition between S100A7 and the turn-on fluorescent Zn(II) sensor Fluozin-3 (FZ3, apparent $K_{d,Zn} = 9$ nM).[38] Because FZ3 exhibits a fluorescent response to Ca(II), these titrations were performed in the absence of Ca(II). With the exception of $S100A7\Delta_{ox,}$ negligible change in FZ3 emission was observed following addition of 2 μM Zn(II) to solutions containing 2 μM of FZ3 and 2 μM S100A7 (Figure 6). This result indicates that S100A7 coordinates Zn(II) with higher affinity than FZ3. In contrast, fluorescent turn-on comparable to the FZ3-only control was observed in the presence of $S100A7\Delta_{ox}$, confirming the importance of the His_3Asp sites in Zn(II) coordination.

We next conducted competition experiments by using a higher-affinity and Ca(II)-insensitive turn-on fluorescent Zn(II) sensor, Zinpyr-4 (ZP4, apparent $K_{d,Zn} = 650$ pM).[39] In

preliminary studies, we observed that ZP4 and the S100A7 proteins competed for Zn(II) in both the absence and presence of Ca(II). We therefore titrated Zn(II) into mixtures containing 5 μM S100A7 and 2 μM ZP4 (75 mM HEPES, 100 mM NaCl, pH 7.0) and fit the resulting data to obtain apparent $K_{d,Zn}$ values (Figures 7, S15–S18, Table S4). Because S100A7 is a homodimer with two identical His_3Asp sites, we focus on a two-site binding model where $K_{d1} = K_{d2}$. Nevertheless, during our analyses, we also fit the data using a one-site model and a two-site binding model where $K_{d1} \neq K_{d2}$ for the purpose of comparison (Table S4). We also simulated fits using K_d values that are 2- to 10-fold lower and 2- to 10-fold higher than the values we ascertained; these simulations support the validity of the reported fits (Figure S19).

The dataset obtained from the ZP4 competitions yields several noteworthy observations. For the four S100A7 species examined, the apparent $K_{d,Zn}$ values obtained from data fitting are all within one order of magnitude, ranging from 430–700 pM and 370–580 pM in the absence and presence of excess Ca(II) ions, respectively (Table 4Figure 7). These results indicate that (i) the absence or presence of the Cys47–Cys96 disulfide bond in each S100A7 subunit has negligible impact on the apparent $K_{d,Zn}$ and (ii) the Ca(II)-free and Ca(II)-bound forms of S100A7 have similar Zn(II) affinities. We note that the titration curves for $S100A7_{ox}$ obtained in the absence and presence of Ca(II) are similar and suggest that Ca(II) may slightly reduce the Zn(II)- binding affinity (Figure 7A), whereas the corresponding titration curves for $S100A7_{red}$, S100A7-Ser, and S100A7-Ala show the opposite trend where the presence of Ca(II) ions shift the titration curve to the right, indicating slightly higher affinity binding (Figure 7B–D). These comparisons also suggest that Ca(II) binding has greater influence on S100A7 when the Cys47–Cys96 disulfide bond is reduced or removed by site-directed mutagenesis. Although the Ca(II)-induced perturbations observed by ZP4 is small, and arguably not functionally significant, it appears that Ca(II) binding to S100A7 slightly enhances the Zn(II)-binding affinity when the Cys47–Cys96 disulfide bond is absent. The overall conclusion from this dataset – a minor effect of Ca(II) ions on the Zn(II)-binding affinities for S100A7 – differs from what is observed for calprotectin (S100A8/S100A9 oligomer). In general, the metal-binding affinities of calprotectin increase by at least several orders of magnitude in the presence of excess Ca(II) ions.[40,41] Lastly, the results from the Zn(II) competition experiments and the apparent $K_{d,Zn}$ values obtained using ZP4 are contrary to the $K_{d,Zn}$ value of 100 μM for S100A7 that was previously reported from equilibrium dialysis studies.[8]

Human S100A7 Selectively Depletes Zn(II) From Bacterial Growth Medium

With information about the Zn(II):S100A7 stoichiometries and support for high-affinity Zn(II) binding in hand, we performed a series of metal-depletion experiments to ascertain which metal(s) S100A7 depletes from microbial growth media following an established procedure.[42] We treated TSB:Tris growth medium, which has been routinely employed in microbiology studies of related S100 proteins (e.g. calprotectin, S100A12),[27,40,41,43,44] with S100A7 (0–500 μg/mL) for 20 h at 30 °C and then separated the protein from the treated medium by spin filtration. The concentrations of unbound Mn, Fe, Ni, Cu and Zn in the treated medium were determined by ICP-MS (Figure 8). Because of the spin filtration step, which can disrupt a mixture at equilibrium, these experiments provide information about the

metal ions that are likely to be sequestered by S100A7 rather than an equilibrium measurement.

The TSB:Tris medium prepared in our laboratory contains approximately 5 μM Zn, 3 μM Fe, 200 nM Mn, 600 nM Ni, and 150 nM Cu (Table S5, Figure 8). We observed that $S100A7_{ox}$, S100A7-Ser and S100A7-Ala depleted Zn from the medium in a concentration-dependent manner, whereas the concentrations of the other transition metal ions were largely unperturbed (Figures 8 and S20, Table S5–S20). Moreover, the presence of a 2-mM Ca(II) supplement had negligible effect on the metal depletion profile of each protein. These results illuminate two keys points: (i) the absence or presence of 2 mM Ca(II) and (ii) the presence or absence of the disulfide bond do not significantly impact the ability of S100A7 to deplete Zn from TSB:Tris medium. Both observations are reminiscent of the ZP4 competition experiments, which indicate similar apparent $K_{d,Zn}$ values for all proteins tested under conditions of low and high Ca(II) (Table S4). In general, the metal-depletion profile of S100A7 is similar to that of S100A12, which selectively depletes Zn(II) from TSB:Tris medium.[41] However, one major difference is that the presence of excess Ca(II) ions enhances Zn(II) depletion by S100A12.

Evidence for a Contribution of the Intramolecular Disulfide Bonds to Antibacterial Activity

We next evaluated the antibacterial activity of $S100A7_{ox}$, S100A7-Ser and S100A7-Ala against *E. coli* K-12 and the Δ*znuA* mutant obtained from the Keio Collection[45] (Figure 9, Table S21). The ATP-binding cassette transport system ZnuABC is a high-affinity Zn(II) uptake system of *E. coli*.[46] ZnuA is the periplasmic Zn(II)-binding protein that delivers Zn(II) to the inner membrane transporter ZnuBC. *E. coli* that lack functional ZnuABC are more susceptible to Zn(II) deprivation compared to the parent strain.[46] We previously used the Δ*znuA* mutant as tool for probing Zn(II) sequestration by human S100A12,[41] and reasoned that experiments with this mutant would inform our understanding of S100A7. Thus, we investigated the growth inhibitory activity of $S100A7_{ox}$, S100A7-Ser and S100A7-Ala under conditions routinely used to study metal-sequestering host-defense proteins such as calprotectin and S100A12.[27,40,41,43,44] We employed TSB:Tris medium with and without a 2-mM Ca(II) supplement. These conditions differ from the majority of experiments that report on the antimicrobial activity of S100A7 and employ phosphate buffer supplemented with 1% growth medium.[10–12,15] We did not consider $S100A7_{red}$ in these assays because $S100A7_{red}$ converted to $S100A7_{ox}$ during the 20-h incubation in TSB:Tris medium, even in the presence of an exogenous reducing agent (Figure S21).

Under these assay conditions, untreated *E. coli* K-12 grew to an OD_{600} ≈0.45. Treatment of *E. coli* K-12 with 1000 μg/mL (40 μM) $S100A7_{ox}$ resulted in some growth inhibition at the 8-h time point (OD_{600} ≈0.2, ±Ca), but full growth was observed at the 20-h time point (Figure 9A). The presence of 1000 μg/mL S100A7-Ser or S100A7-Ala had negligible effect on *E. coli* growth. In contrast, all three proteins inhibited growth of the Δ*znuA* mutant (Figure 9B). Whereas full growth inhibition occurred following treatment with 1000 μg/mL $S100A7_{ox}$, the S100A7-Ser and S100A7-Ala variants inhibited growth to a lesser degree at the 20-h time point (OD_{600} ≈0.2). The 2-mM Ca(II) supplement had negligible effect in all cases. Taken together, these results indicate that ZnuABC can outcompete S100A7 for Zn(II)

under these growth conditions. The data also suggest that, in the absence of a functional ZnuABC transport system, $S100A7_{ox}$ is more effective than the disulfide-null variants at inhibiting *E. coli* growth.

To further evaluate the *in vitro* antibacterial activity of S100A7, we screened the growth inhibitory activity of $S100A7_{ox}$ and variants against five additional bacterial strains. On the basis of prior antimicrobial activity studies of S100A7[10] as well as S100A12[41, 44] and calprotectin,[40,42,44,47] we selected *E. coli* ATCC 25922, *Pseudomonas aeruginosa* PAO1, *Staphylococcus aureus* ATCC 25923, *Listeria monocytogenes* ATCC 19115, and *Lactobacillus plantarum* WSCF1 (Table S21). We treated bacteria with 1000 μg/mL protein and monitored growth by OD_{600} following a 20-h incubation (Figure 10). In general, the presence of S100A7 had negligible effect on the OD_{600} values for the *E. coli*, *P. aeruginosa*, and *S. aureus* strains, although slight growth inhibition was observed for *P. aeruginosa* treated with $S100A7_{ox}$. Growth of *L. monocytogenes* and *L. plantarum* was inhibited upon treatment with $S100A7_{ox}$ in the absence and presence of a 2-mM Ca(II) supplement, respectively. In contrast, S100A7-Ser, S100A7-Ala, and $S100A7\Delta_{ox}$ did not inhibit the growth of these two microbes.

A comparison of these data to the results from prior studies of the antimicrobial activity of S100A12 and calprotectin is informative. S100A12 contains two His_3Asp sites at the dimer interface and sequesters Zn(II),[41] whereas calprotectin harbors one His_3Asp and one His_6 site.[44,48] The latter site allows calprotectin to sequester multiple first-row transition metals.[42] This work shows that the antibacterial activity spectrum of $S100A7_{ox}$ is similar to that of S100A12. Under the assay conditions employed in this work, both proteins exhibit growth inhibitory activity against *E. coli* Δ*znuA, L. monocytogenes*, and *L. plantarum* but not *P. aeruginosa, S. aureus*, and *E. coli* K-12. A caveat to this comparison is that the lack of a Ca(II) effect for S100A7 observed in this work and also by others[10,11,13], which differs from the Ca(II)-enhanced antimicrobial activity reported for S100A12.[41] In contrast to $S100A7_{ox}$ and S100A12, calprotectin displays growth inhibitory activity against all of the bacterial species considered in this work.[40,42,44,47] Both $S100A7_{ox}$ and S100A12 are selective and sequester Zn(II), whereas calprotectin is versatile and sequesters multiple divalent first-row transition metal ions (e.g. Mn, Fe, Ni, Zn). Thus, it is likely that organisms that exhibit inhibited growth in the presence of $S100A7_{ox}$ and S100A12 are less able to compete with Zn(II)-chelating proteins for this metal ion and more susceptible to Zn(II) deprivation, at least under the growth conditions employed in this work, than the strains that are resistant to these proteins.

Under the antibacterial assay conditions employed in this work, we observed negligible growth inhibition of *E. coli* K-12 and ATCC 25922 by S100A7. Prior studies of S100A7 have reported that S100A7 possesses antibacterial activity against *E. coli.*[10] These contrasting outcomes likely result from different experimental conditions employed in the current work and previous studies, and suggest that S100A7 exerts condition-dependent antimicrobial activity. Previous assays employed a microdilution assay in which *E. coli* cultures (10^4 – 10^5 CFU/mL) were incubated in 10 mM phosphate buffer containing 1% growth medium (e.g. TSB or LB) and treated with S100A7 for 3 h at 37 °C, followed by serial dilution and plating on agar. We performed this microdilution assay with $S100A7_{ox}$,

and consistent with prior work, we observed a ≈2-log fold reduction in the CFU/mL of *E. coli* K-12 and ATCC 25922 when the cultures were treated with 1000 μg/mL (≈40 μM) of protein (Figure S22). We tentatively propose that S100A7 exhibits different antimicrobial mechanisms under different assay conditions, and evaluating this notion is an avenue for future work.

The Redox State of Human S100A7 Influences Metal Displacement at the His_3Asp Sites

Overall, our studies of Zn(II) binding and metal depletion reveal that $S100A7_{ox}$ and the disulfide-null variants display similar Zn(II) competition with ZP4 and Zn(II) selectivity. However, the antibacterial activity assays suggest that $S100A7_{ox}$ is more effective at Zn(II) sequestration than the disulfide-null variants. To address this matter further, we interrogated the metal-binding properties of S100A7 by monitoring Co(II) binding and probing metal substitution at the His_3Asp sites by using Co(II) as a spectroscopic probe. We first performed Co(II)-binding titrations in the absence and presence of excess Ca(II). In all cases, solutions of S100A7 changed from colorless to pink upon addition of Co(II). The optical absorption spectra of the Co(II)-S100A7 variants exhibited *d*–*d* transitions centered at 563 nm ($\Sigma_{563} \approx 500$ to 580 $M^{-1}cm^{-1}$) (Figure 11). This spectroscopic signature is similar to the Co(II)-bound His_3Asp sites of human calprotectin and S100A12.[40,41] During each Co(II)-binding titration, the absorbance at 563 nm increased until ≈2 equivalents of Co(II) were added, indicating the expected 2:1 Co(II):S100A7 stoichiometry (Figure 11).

We subsequently examined metal substitution at the His_3Asp sites of S100A7 by monitoring the displacement of Co(II) from Co(II)-S100A7 following Zn(II) addition. On the basis of our prior Co(II)-binding studies of calprotectin[40] and S100A12,[41] as well as the Irving-Williams series,[49] we expected that the His_3Asp sites have thermodynamic preference for Zn(II) over Co(II). Addition of Zn(II) to a solution of Co(II)-$S100A7_{ox}$ resulted in a gradual color change from pink to colorless, and loss of the absorbance feature centered at 563 nm, consistent with loss of Co(II) from the His_3Asp sites and formation of Zn(II)-bound $S100A7_{ox}$ (Figure 12). After a 20-h incubation at room temperature, ≈20% of $S100A7_{ox}$ remained Co(II) bound. In contrast, addition of Zn(II) to Co(II)-$S100A7_{red}$ resulted in a comparatively rapid loss of Co(II) from the His_3Asp sites (Figure 12). A comparison of the spectra obtained at the 1-h time point indicates almost complete metal substitution for $S100A7_{red}$ whereas ≈80% of $S100A7_{ox}$ remains Co(II) bound. This difference in metal substitution occurred both in the absence and presence of Ca(II). Addition of Zn(II) to Co(II)-S100A7-Ser and Co(II)-S100A7-Ala afforded trends similar to that of $S100A7_{red}$ (Figure 12). These results suggest that the disulfide bond decreases the kinetic lability of Co(II) ions bound to S100A7. It is possible that the Cys47–Cys96 disulfide bond limits the conformational flexibility of the S100A7 C-terminus, which pre-organize the His_3Asp binding site or stabilizes the Co(II)-bound form of the protein. Since Zn(II) and Co(II) bind to the same His_3Asp sites of S100A7, it is also possible that a similar trend occurs for Zn(II)-bound S100A7 with $S100A7_{ox}$ more effectively entrapping the Zn(II) ion than $S100A7_{red}$.

Furthermore, we noted a subtle but reproducible effect of Ca(II) addition for variants where the Cys47–Cys96 disulfide bond is reduced or removed by site-directed mutagenesis. For

instance, an inspection of the spectra obtained 20 min after Zn(II) addition reveals that the absorbance signal corresponding to Co(II) binding was weaker in the absence of Ca(II) compared to the samples containing Ca(II) for $S100A7_{red}$, S100A7-Ser, and S100A7-Ala. This observation indicates that the Co(II) ion bound to these protein species is less readily substituted by Zn(II) when Ca(II) ions are present. This behavior is reminiscent of the ZP4 titration curves of $S100A7_{red}$, S100A7-Ser, and S100A7-Ala which indicated slightly higher Zn(II) binding affinity in the presence of excess Ca(II) (Figure 7B–D). Together, these data suggest that Ca(II) binding provides some enhancement of transition-metal-binding affinities at the His_3Asp sites when the disulfide bond is not present.

Summary and Outlook

In this work, we have examined the interplay between disulfide-bond redox chemistry, Zn(II)-binding properties, and antibacterial activity of human S100A7. Our studies provide several insights about the structure and antibacterial role of this protein and illuminate avenues for further exploration. The current data indicate that Ca(II) ions affect the redox behavior of the Cys47–Cys96 disulfide bond. By depressing the E_m value, Ca(II) binding causes the disulfide bond to be more difficult to reduce, and this phenomenon may be relevant to *in vivo* speciation and physiological function(s) of S100A7. In particular, the antibacterial activity assays and metal substitution experiments provide clues that $S100A7_{ox}$ and $S100A7_{red}$ exhibit differing metal-sequestering abilities with the oxidized protein showing enhanced antimicrobial activity against *E. coli* Δ*znuA* and relatively slow metal substitution at the His_3Asp sites. S100A7 is a cytoplasmic protein that is released from epithelial cells into the extracellular milieu where Ca(II) levels are orders of magnitude higher than those found in the cytoplasm.[25, 26] Hence, we reason that Ca(II)-bound S100A7 exists in the extracellular space. It is conceivable that the high Ca(II) levels in this environment favor the formation and persistence of $S100A7_{ox}$, tuning the Zn(II)-binding and antibacterial properties of this protein for optimal function. We also observed that Zn(II) coordination impedes disulfide bond reduction; this behavior may indicate another related strategy that S100A7 uses to ensure that Zn(II) remains bound. Whether Ca(II) or Zn(II) binding facilitates the oxidation of $S100A7_{red}$ to $S100A7_{ox}$ and persistence of the latter species *in vivo* merits investigation. It is also possible that metals ions and disulfide bond formation have additional and as-yet unexplored consequences for S100A7. For example, Ca(II) and transition metal binding confers protease resistance to human calprotectin,[50] and it is possible that metal binding and disulfide bond formation influence the stability and biological lifetime of S100A7 by modulating its proteolytic susceptibility. Moreover, the complex speciation of S100A7 may provide this protein with as-yet unappreciated functional versatility.

The ideas presented above differ from a model presented recently that focuses on $S100A7_{red}$.[12] Both $S100A7_{ox}$ and $S100A7_{red}$ have been isolated from samples of human skin, and in this prior work, $S100A7_{red}$ was identified as an antifungal component of lesion psoriasis scale extracts.[10,12] Subsequent antifungal susceptibility testing indicated that $S100A7_{red}$ has greater antifungal activity than $S100A7_{ox}$.[12] The epidermis contains high levels of thioredoxin and thioredoxin reductase,[5152] and $S100A7_{ox}$ was shown to be a substrate for the thioredoxin system *in vitro,* providing a potential mechanism for $S100A7_{red}$

to persist in the extracellular space and confer antifungal activity.[12] Our results suggest that metal-bound $S100A7_{ox}$ is not readily reduced by the thioredoxin system, and that apo $S100A7_{ox}$ can be effective at inhibiting bacterial growth than $S100A7_{red}$.

Several different antimicrobial mechanisms for S100A7 have been proposed that include Zn(II) withholding,[10,12] bacterial membrane permeabilization,[15] and a contribution to epithelial barrier protection by forming cross-links and cellular adherence.[13] A comparison of the current antibacterial activity assays and prior studies reveal differences in experimental outcomes depending on the assay conditions. Although the current results support a role for S100A7 in the human Zn(II)-withholding response, further studies are required to investigate this putative function and additional antimicrobial mechanisms that may be at work. We note that there is no murine orthologue of S100A7, which limits the utility of murine model of infection for studying this protein.

The molecular basis for bacterial membrane disruption by S100A7 is unclear, and whether metal ions influence this activity remains largely unexplored. Metal ions have been shown to modulate the antimicrobial activity of other peptides that damage membranes. For example, clavanin A is a Zn(II)-binding peptide expressed by the tunicate *Styela clava* that displays enhanced pore-forming activity against *E. coli* in the presence of Zn(II).[53] It is possible that Ca(II) and Zn(II) binding modulate the ability of S100A7 to damage membranes, and further explorations of a link between metals ions and this bactericidal mode of action are warranted.

In closing, the results presented herein inform our understanding of the S100 protein family and highlight key differences between human S100A7, S100A12, and calprotectin (*vide supra*), three abundant metal-chelating human host-defense proteins. Although each protein binds Ca(II) ions at EF-hand domains, the consequences of Ca(II) ion coordination differ. Ca(II) ions modulate the quaternary structure, metal-binding properties, and antimicrobial activity of calprotectin[40,42,54–57] and S100A12,[41,58] whereas Ca(II) ions appear to have negligible influence on these three properties for S100A7. Instead, Ca(II) ions affect the redox behavior of the intramolecular disulfide bonds in S100A7. Nevertheless, our data suggest that this effect may provide a means for enhancing Zn(II) chelation and antibacterial activity through nutrient deprivation in the extracellular space.

Supplementary Material

Refer to Web version on PubMed Central for supplementary material.

Acknowledgments

Funding Source Statement

This work was supported by the NSF (CHE-1352132), the MIT Department of Chemistry, and the MIT Undergraduate Research Opportunities Program (UROP, funding to G.E.R. and H.A.F.). The MIT Biophysical Instrumentation Facility for the Study of Complex Macromolecular Systems is supported by NSF grant 0070319. The ICP-MS instrument is housed in the MIT Center for Environmental Health Sciences Bioanalytical Core, which is supported by NIH grant P30-ES002109.

The *E. coli* K-12 and Δ*znuA* strains were obtained from the Keio Collection.[45]

Abbreviations

AEC	anion-exchange chromatography
ATCC	American Type Culture Collection
CD	circular dichroism
DTT	1,4-dithiothreitol
DTDP	4,4′-dithiodipyridine
GSH	reduced glutathione
GSSG	oxidized glutathione
$HD5_{ox}$	oxidized human defensin 5
HEPES	4-(2-hydroxyethyl)-1-piperazineethanesulfonic acid
HPLC	high performance liquid chromatography
SDM	standard deviation of the mean
SEC	size-exclusion chromatography
$S100A7_{ox}$	oxidized S100A7 with Cys47–Cys96 disulfide bond
$S100A7_{red}$	reduced S100A7 with Cys47 and Cys96 as free thiols
S100A7-Ser	S100A7(C47S)(C96S) homodimer
S100A7-Ala	S100A7(C47A)(C96A) homodimers
$S100A7\Delta_{ox}$	S100A7(H18A)(H87A)(H91A)(D25A) oxidized with Cys47–Cys96 disulfide bond
Tris	tris(hydroxymethyl)aminomethane
Trx	thioredoxin
TrxR	thioredoxin reductase

References

1. Grice EA, Segre JA. The skin microbiome. Nat Rev Microbiol. 2011; 9:244–253. [PubMed: 21407241]
2. Diamond G, Beckloff N, Weinberg A, Kisich KO. The roles of antimicrobial peptides in innate host defense. Curr Pharm Des. 2009; 15:2377–2392. [PubMed: 19601838]
3. McCormick TS, Weinberg A. Epithelial cell-derived antimicrobial peptides are multifunctional agents that bridge innate and adaptive immunity. Periodontol 2000. 2010; 54:195–206. [PubMed: 20712640]
4. Madsen P, Rasmussen HH, Leffers H, Honoré B, Dejgaard K, Olsen E, Kiil J, Walbum E, Andersen AH, Basse B, Lauridsen JB, Ratz GP, Celis A, Vanderkeckhove J, Celis JE. Molecular cloning, occurrence, and expression of a novel partially secreted protein “psoriasin” that is highly upregulated in psoriatic skin. J Invest Dermatol. 1991; 97:701–712. [PubMed: 1940442]

5. Hoffmann HJ, Olsen E, Etzerodt M, Madsen P, Thøgersen HC, Kruse T, Celis JE. Psoriasin binds calcium and is upregulated by calcium to levels that resemble those observed in normal skin. J Invest Dermatol. 1994; 103:370–375. [PubMed: 8077703]
6. Brodersen DE, Nyborg J, Kjeldgaard M. Zinc-binding site of an S100 protein revealed. Two crystal structures of Ca2+-bound human psoriasin (S100A7) in the Zn2+-loaded and Zn2+-free states. Biochemistry. 1999; 38:1695–1704. [PubMed: 10026247]
7. Tan JQ, Vorum H, Larsen CG, Madsen P, Rasmussen HH, Gesser B, Etzerodt M, Honoré B, Celis JE, Thestrup-Pedersen K. Psoriasin: A novel chemotactic protein. J Invest Dermatol. 1996; 107:5–10. [PubMed: 8752830]
8. Vorum H, Madsen P, Rasmussen HH, Etzerodt M, Svendsen I, Celis JE, Honoré B. Expression and divalent cation binding properties of the novel chemotactic inflammatory protein psoriasin. Electrophoresis. 1996; 17:1787–1796. [PubMed: 8982613]
9. Wolf R, Ruzicka T, Yuspa SH. Novel S100A7 (psoriasin)/S100A15 (koebnerisin) subfamily: highly homologous but distinct in regulation and function. Amino Acids. 2011; 41:789–796. [PubMed: 20596736]
10. Gläser R, Harder J, Lange H, Bartels J, Christophers E, Schröder JM. Antimicrobial psoriasin (S100A7) protects human skin from *Escherichia coli* infection. Nat Immunol. 2005; 6:57–64. [PubMed: 15568027]
11. Mildner M, Stichenwirth M, Abtin A, Eckhart L, Sam C, Gläser R, Schröder JM, Gmeiner R, Mlitz V, Pammer J, Geusau A, Tschachler E. Psoriasin (S100A7) is a major antimicrobial component of the female genital tract. Mucosal Immunol. 2010; 127:602–609.
12. Hein KZ, Takahashi H, Tsumori T, Yasui Y, Nanjoh Y, Toga T, Wu ZH, Grötzinger J, Jung S, Wehkamp J, Schroeder BO, Schroeder JM, Morita E. Disulphide-reduced psoriasin is a human apoptosis-inducing broad-spectrum fungicide. Proc Natl Acad Sci U S A. 2015; 112:13039–13044. [PubMed: 26438863]
13. Meyer JE, Harder J, Sipos B, Maune S, Klöppel G, Bartels J, Schröder JM, Gläser R. Psoriasin (S100A7) is a principal antimicrobial peptide of the human tongue. Mucosal Immunol. 2008; 1:239–243. [PubMed: 19079183]
14. Lee KC, Eckert RL. S100A7 (Psoriasin) - Mechanism of antibacterial action in wounds. J Invest Dermatol. 2007; 127:945–957. [PubMed: 17159909]
15. Michalek M, Gelhaus C, Hecht O, Podschun R, Schröder JM, Leippe M, Grötzinger J. The human antimicrobial protein psoriasin acts by permeabilization of bacterial membranes. Dev Comp Immunol. 2009; 33:740–746. [PubMed: 19162067]
16. Weinberg ED. Nutritional immunity: Host's attempt to withhold iron from microbial invaders. J Am Med Assoc. 1975; 231:39–41.
17. Hood MI, Skaar EP. Nutritional immunity: transition metals at the pathogen–host interface. Nat Rev Microbiol. 2012; 10:525–537. [PubMed: 22796883]
18. Matthijs S, Hernalsteens JP, Roelants K. An orthologue of the host-defense protein psoriasin (S100A7) is expressed in frog skin. Dev Comp Immunol. 2017; 67:395–403. [PubMed: 27569988]
19. Gifford JL, Walsh MP, Vogel HJ. Structures and metal-ion-binding properties of the Ca2+-binding helix-loop-helix EF-hand motifs. Biochem J. 2007; 405:199–221. [PubMed: 17590154]
20. Brodersen DE, Etzerodt M, Madsen P, Celis JE, Thøgersen HC, Nyborg J, Kjeldgaard M. EF-hands at atomic resolution: the structure of human psoriasin (S100A7) solved by MAD phasing. Structure with Folding & Design. 1998; 6:477–489. [PubMed: 9562557]
21. Mely Y, Gerard D. Structural and ion-binding properties of an S100b protein mixed disulfide: comparison with the reappraised native S100b protein properties. Arch Biochem Biophys. 1990; 279:174–182. [PubMed: 2337349]
22. Mely Y, Gerard D. Intra- and interchain disulfide bond generation in S100b protein. J Neurochem. 1990; 55:1100–1106. [PubMed: 2398350]
23. Matsui Lee IS, Suzuki M, Hayashi N, Hu J, Van Eldik LJ, Titani K, Nishikimi M. Copper-dependent formation of disulfide-linked dimer of S100B protein. Arch Biochem Biophys. 2000; 374:137–141. [PubMed: 10666291]

24. Scotto C, Mély Y, Ohshima H, Garin J, Cochet C, Chambaz E, Baudier J. Cysteine oxidation in the mitogenic S100B protein leads to changes in phosphorylation by catalytic CKII-alpha subunit. J Biol Chem. 1998; 273:3901–3908. [PubMed: 9461574]
25. Williams RJP. Calcium binding proteins in normal and transformed cells, Perugia, May 1996. Cell Calcium. 1996; 20:87–93. [PubMed: 8864575]
26. Brini M, Ottolini D, Cali T, Carafoli E. Calcium in health and disease. Met Ions Life Sci. 2013; 20:87–93.
27. Brophy MB, Nakashige TG, Gaillard A, Nolan EM. Contributions of the S100A9 C-terminal tail to high-affinity Mn(II) chelation by the host-defense protein human calprotectin. J Am Chem Soc. 2013; 135:17804–17817. [PubMed: 24245608]
28. Smith RC, Reed VD. Inhibition by thiols of copper(II)-induced oxidation of oxihemoglobin. Chem Biol Interact. 1992; 82:209–217. [PubMed: 1568271]
29. Lundström J, Holmgren A. Determination of the reduction oxidation potential of the thioredoxin-like domains of protein disulfide-isomerase from the equilibrium with glutathione and thioredoxin. Biochemistry. 1993; 32:6649–6655. [PubMed: 8329391]
30. Harrison CA, Raftery MJ, Walsh J, Alewood P, Iismaa SE, Thliveris S, Geczy CL. Oxidation regulates the inflammatory properties of the murine S100 protein S100A8. J Biol Chem. 1999; 274:8561–8569. [PubMed: 10085090]
31. Sokołowska M, Bal W. Cu(II) complexation by “non-coordinating” N-2-hydroxyethylpiperazine-N′-2-ethanesulfonic acid (HEPES buffer). J Inorg Biochem. 2005; 99:1653–1660. [PubMed: 15993944]
32. Holmgren A. Thioredoxin. Ann Rev Biochem. 1985; 54:237–271. [PubMed: 3896121]
33. Go YM, Jones DP. Redox compartmentalization in eukaryotic cells. Biochimica Et Biophysica Acta-General Subjects. 2008; 1780:1271–1290.
34. Åslund F, Berndt KD, Holmgren A. Redox potentials of glutaredoxins and other thiol-disulfide oxidoreductases of the thioredoxin superfamily determined by direct protein-protein redox equilibria. J Biol Chem. 1997; 272:30780–30786. [PubMed: 9388218]
35. Zhang YF, Cougnon FBL, Wanniarachchi YA, Hayden JA, Nolan EM. Reduction of human defensin 5 affords a high-affinity zinc-chelating peptide. ACS Chem Biol. 2013; 8:1907–1911. [PubMed: 23841778]
36. Talmard C, Bouzan A, Faller P. Zinc binding to amyloid-beta: Isothermal titration calorimetry and Zn competition experiments with Zn sensors. Biochemistry. 2007; 46:13658–13666. [PubMed: 17983245]
37. Maret W, Vallee BL. Thiolate ligands in metallothionein confer redox activity on zinc clusters. Proc Natl Acad Sci U S A. 1998; 95:3478–3482. [PubMed: 9520391]
38. Krężel A, Maret W. Dual nanomolar and picomolar Zn(II) binding properties of metallothionein. J Am Chem Soc. 2007; 129:10911–10921. [PubMed: 17696343]
39. Burdette SC, Frederickson CJ, Bu WM, Lippard SJ. ZP4, an improved neuronal Zn2+ sensor of the Zinpyr family. J Am Chem Soc. 2003; 125:1778–1787. [PubMed: 12580603]
40. Brophy MB, Hayden JA, Nolan EM. Calcium ion gradients modulate the zinc affinity and antibacterial activity of human calprotectin. J Am Chem Soc. 2012; 134:18089–18100. [PubMed: 23082970]
41. Cunden LS, Gaillard A, Nolan EM. Calcium ions tune the zinc-sequestering properties and antimicrobial activity of human S100A12. Chemical Science. 2016; 7:1338–1348. [PubMed: 26913170]
42. Nakashige TG, Zhang B, Krebs C, Nolan EM. Human calprotectin is an iron-sequestering host-defense protein. Nat Chem Biol. 2015; 11:765–771. [PubMed: 26302479]
43. Kehl-Fie TE, Chitayat S, Hood MI, Damo S, Restrepo N, Garcia C, Munro Kim A, Chazin WJ, Skaar EP. Nutrient metal sequestration by calprotectin inhibits bacterial superoxide defense, enhancing neutrophil killing of *Staphylococcus aureus*. Cell Host Microbe. 2011; 10:158–164. [PubMed: 21843872]
44. Damo SM, Kehl-Fie TE, Sugitani N, Holt ME, Rathi S, Murphy WJ, Zhang YF, Betz C, Hench L, Fritz G, Skaar EP, Chazin WJ. Molecular basis for manganese sequestration by calprotectin and

roles in the innate immune response to invading bacterial pathogens. Proc Natl Acad Sci U S A. 2013; 110:3841–3846. [PubMed: 23431180]

45. Baba T, Ara T, Hasegawa M, Takai Y, Okumura Y, Baba M, Datsenko KA, Tomita M, Wanner BL, Mori H. Construction of *Escherichia coli* K-12 in-frame, single-gene knockout mutants: the Keio collection. Mol Syst Biol. 2006; 2:20060008.
46. Patzer SI, Hantke K. The ZnuABC high-affinity zinc uptake system and its regulator zur in Escherichia coli. Mol Microbiol. 1998; 28:1199–1210. [PubMed: 9680209]
47. Makthal N, Nguyen K, Do H, Gavagan M, Chandrangsu P, Helmann JD, Olsen RJ, Kumaraswami M. A critical role of zinc importer AdcABC in group A *Streptococcus*-host interactions during infection and its implications for vaccine development. EBioMedicine. 2017; 21:131–141. [PubMed: 28596134]
48. Gagnon DM, Brophy MB, Bowman SEJ, Stich TA, Drennan CL, Britt RD, Nolan EM. Manganese Binding Properties of Human Calprotectin under Conditions of High and Low Calcium: X-ray Crystallographic and Advanced Electron Paramagnetic Resonance Spectroscopic Analysis. J Am Chem Soc. 2015; 137:3004–3016. [PubMed: 25597447]
49. Irving H, Williams RJP. The stability of transition-metal complexes. J Chem Soc. 1953; 138:3192–3210.
50. Stephan JR, Nolan EM. Calcium-induced tetramerization and zinc chelation shield human calprotectin from degradation by host and bacterial extracellular proteases. Chemical Science. 2016; 7:1962–1975. [PubMed: 26925211]
51. Arnér ESJ, Holmgren A. Physiological functions of thioredoxin and thioredoxin reductase. Eur J Biochem. 2000; 267:6102–6109. [PubMed: 11012661]
52. Schallreuter KU, Wood JM. The role of thioredoxin reductase in the reduction of free-radicals at the surface of the epidermis. Biochem Biophys Res Commun. 1986; 136:630–637. [PubMed: 2423087]
53. Juliano SA, Pierce S, deMayo JA, Balunas MJ, Angeles-Boza AM. Exploration of the innate immune system of *Styela clava*: Zn^{2+} binding enhances the antimicrobial activity of the tunicate peptide clavanin A. Biochemistry. 2017; 56:1403–1414. [PubMed: 28226206]
54. Hunter MJ, Chazin WJ. High level expression and dimer characterization of the S100 EF-hand proteins, migration inhibitory factor-related proteins 8 and 14. J Biol Chem. 1998; 273:12427–12435. [PubMed: 9575199]
55. Vogl T, Roth J, Sorg C, Hillenkamp F, Strupat K. Calcium-induced noncovalently linked tetramers of MRP8 and MRP14 detected by ultraviolet matrix-assisted laser desorption/ionization mass spectrometry. J Am Soc Mass Spectrom. 1999; 10:1124–1130. [PubMed: 10536818]
56. Strupat K, Rogniaux H, Van Dorsselaer A, Roth J, Vogl T. Calcium-induced noncovalently linked tetramers of MRP8 and MRP14 are confirmed by electrospray ionization-mass analysis. J Am Soc Mass Spectrom. 2000; 11:780–788. [PubMed: 10976885]
57. Hayden JA, Brophy MB, Cunden LS, Nolan EM. High-Affinity Manganese Coordination by Human Calprotectin Is Calcium-Dependent and Requires the Histidine-Rich Site Formed at the Dimer Interface. J Am Chem Soc. 2013; 135:775–787. [PubMed: 23276281]
58. Moroz OV, Burkitt W, Wittkowski H, He W, Ianoul A, Novitskaya V, Xie J, Polyakova O, Lednev IK, Shekhtman A, Derrick PJ, Bjoerk P, Foell D, Bronstein IB. Both Ca2+ and Zn2+ are essential for S100A12 protein oligomerization and function. BMC Biochem. 2009; 10:11. [PubMed: 19386136]

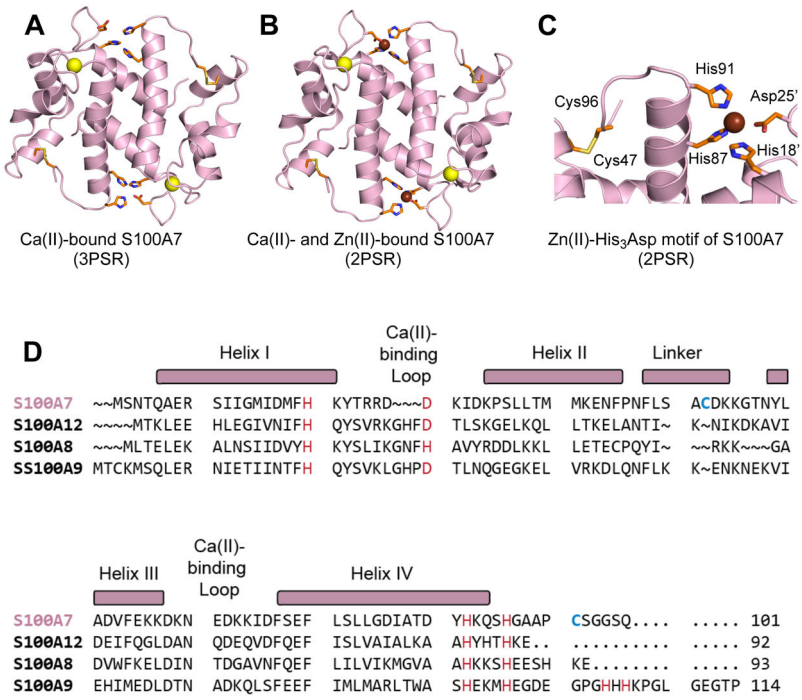

Figure 1.

Crystal structures of human S100A7 and amino acid sequence alignment of S100A7 and select human S100 polypeptides. (A) Structure of the Ca(II)-bound S100A7 homodimer (PDB 3PSR).[6] (B) Structure of the Ca(II)- and Zn(II)-bound S100A7 homodimer (PDB 2PSR).[6] (C) Zoom-in view showing the His_3Asp motif and Cys47–Cys96 disulfide. Ca(II) ions are shown as yellow spheres, and Zn(II) ions as brown spheres. (D) Sequence alignment of human S100A7, human S100A8, human S100A9, and human S100A12. The secondary structural elements presented above the alignment are for human S100A7. The transition-metal binding residues are presented in red and Cys47 and Cys96 of S100A7 are highlighted in blue.

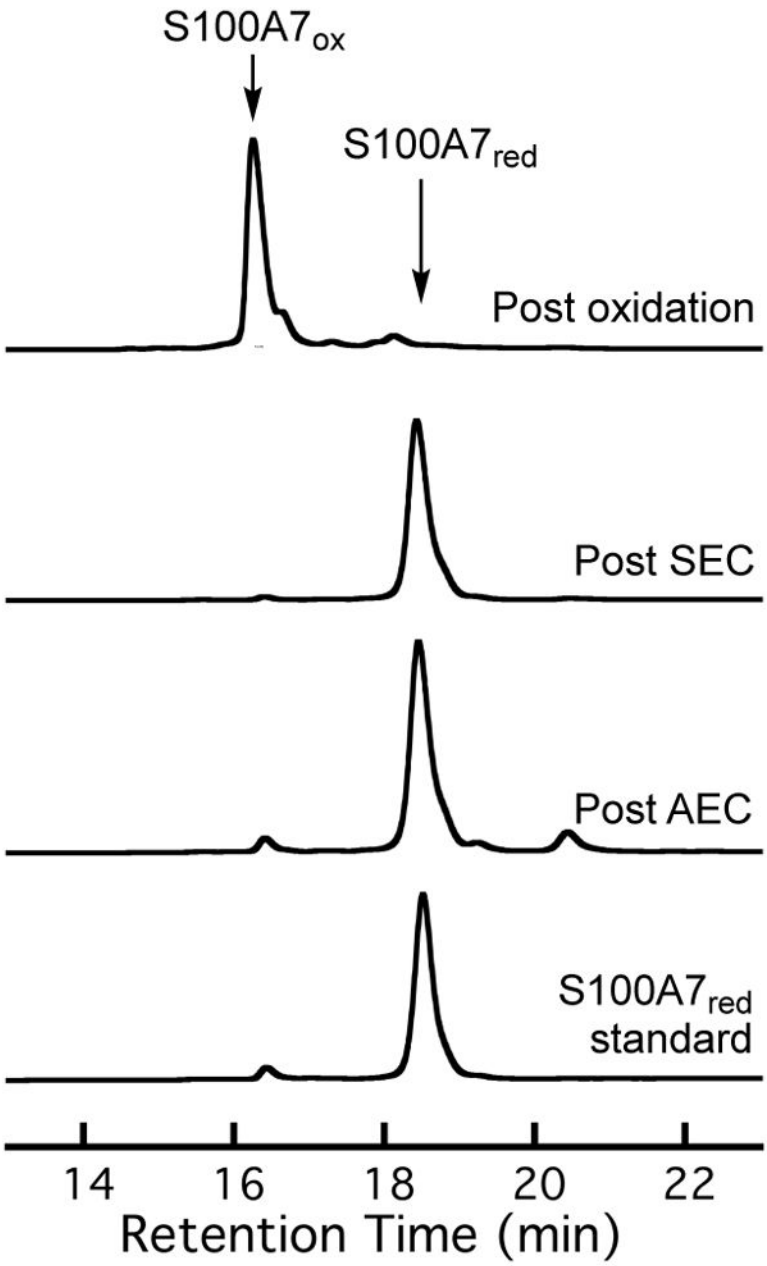

Figure 2.

Analytical HPLC traces (220 nm absorption) showing the speciation of S100A7 (9 μM) after different steps of the protein purification and following Cu(II)-catalyzed oxidation. The protein purification involves purification of S100A7 by AEC and SEC.[27] Each trace was normalized to a maximum peak absorbance of 1. Analytical HPLC traces for S100A7Δ are presented in Figure S1 (Supporting Information). The shoulder peak observed in the chromatograms of S100A7ox corresponds to the isoform of S100A7 missing the N-terminal methionine.

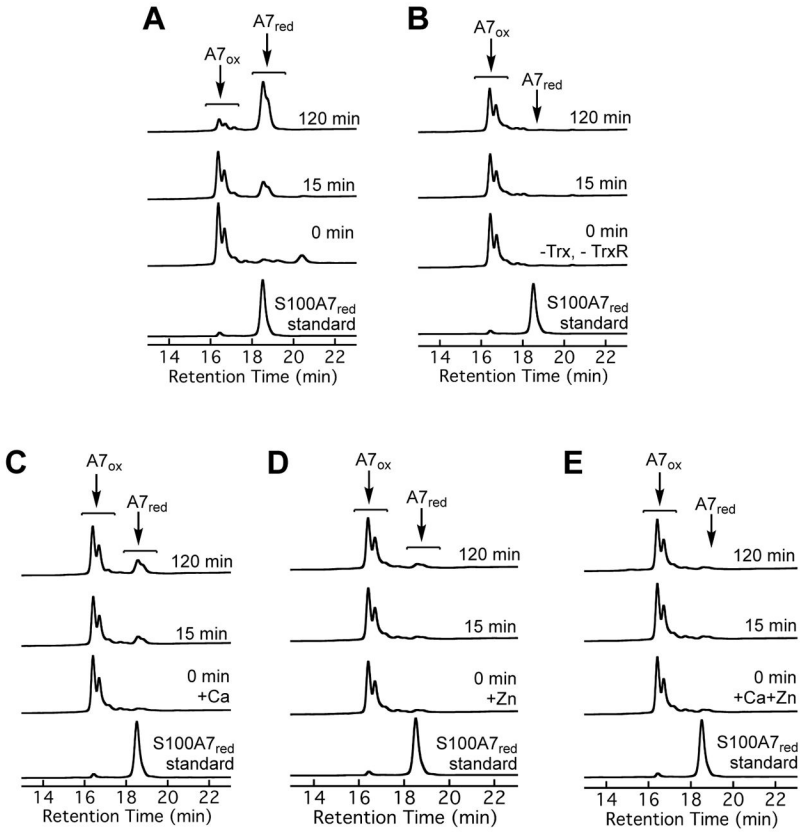

Figure 3.

Analytical HPLC traces (220 nm absorption) from enzymatic activity assays employing the mammalian thioredoxin system and $S100A7_{ox}$ as a substrate. Conditions: 5 μM $S100A7_{ox}$, 1 μM human Trx, 0.1 μM rat liver TrxR, and 1 mM NADPH (75 mM HEPES, 100 mM NaCl, pH 7.0, 37 °C) with (A) no metal added, (B) no enzyme added, (C) 2 mM Ca(II) added to the buffer, (D) 1.9 equiv of Zn(II) added, and (E) 1.9 equiv of Zn(II) and 2 mM Ca(II) added to the buffer. In each panel, the bottom chromatogram is a $S100A7_{red}$ standard. Data from control assays are presented in Figures S6, S8, and S9. The shoulder peaks observed in the chromatograms of S100A7ox and S100A7red correspond to S100A7 isoforms missing the N-terminal methionine.

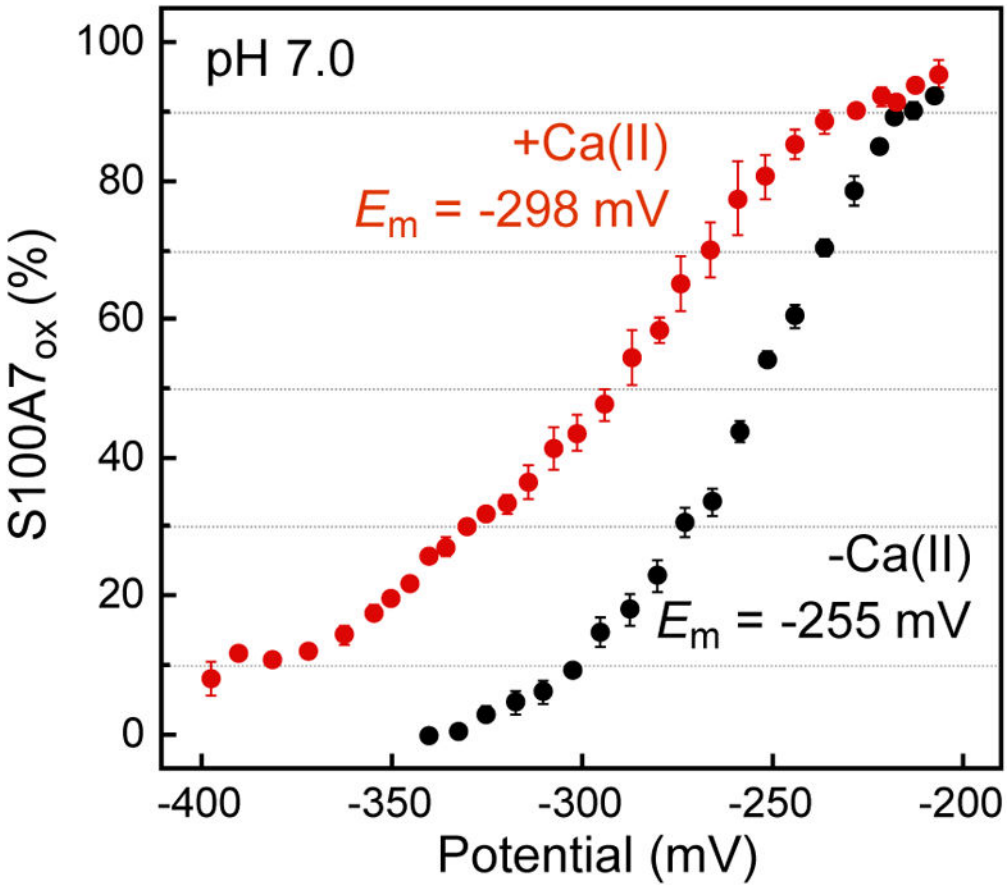

Figure 4.

Ca(II) depresses the midpoint potential of S100A7. Percentage of S100A7$_{ox}$ at equilibrium following incubation of S100A7$_{ox}$ (10 μM) in buffers with defined redox potentials (75 mM HEPES, 100 mM NaCl, pH 7.0, 10 mM total [GSH] and [GSSG], ±2 mM Ca(II)) determined from integration of HPLC peaks (mean ± SDM, n = 3). Black spheres: in the absence of Ca(II); red spheres: in the presence of 2 mM Ca(II). Select HPLC traces are presented in Figure S11.

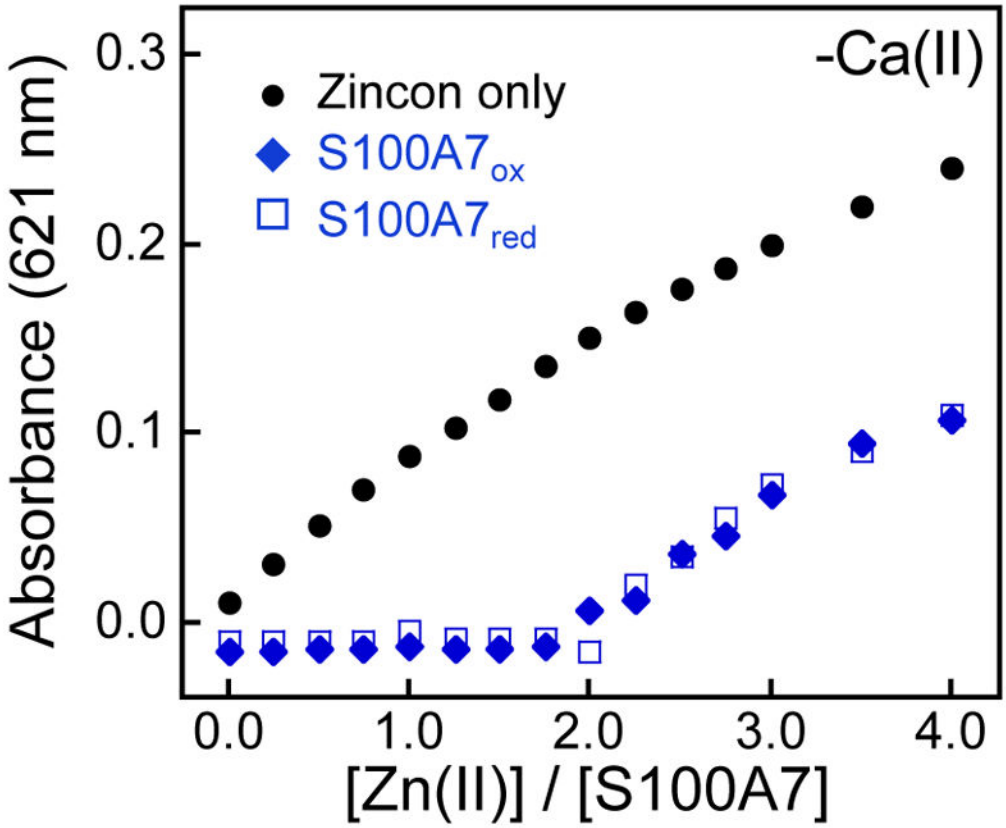

Figure 5.

S100A7 outcompetes Zincon for Zn(II). Representative plots showing the response of 20 μM Zincon to Zn(II) in the presence of 10 μM S100A7 $_{ox}$, S100A7-Ser, S100A7-Ala or S100A7Δ_{ox} in 75 mM HEPES, 100 mM NaCl, pH 7.0, and 25 °C. The Zn(II)-Zincon complex exhibits an absorbance maximum at 621 nm. Data from titrations performed in the presence of Ca(II) and with the disulfide-null variants are presented in Figure S14.

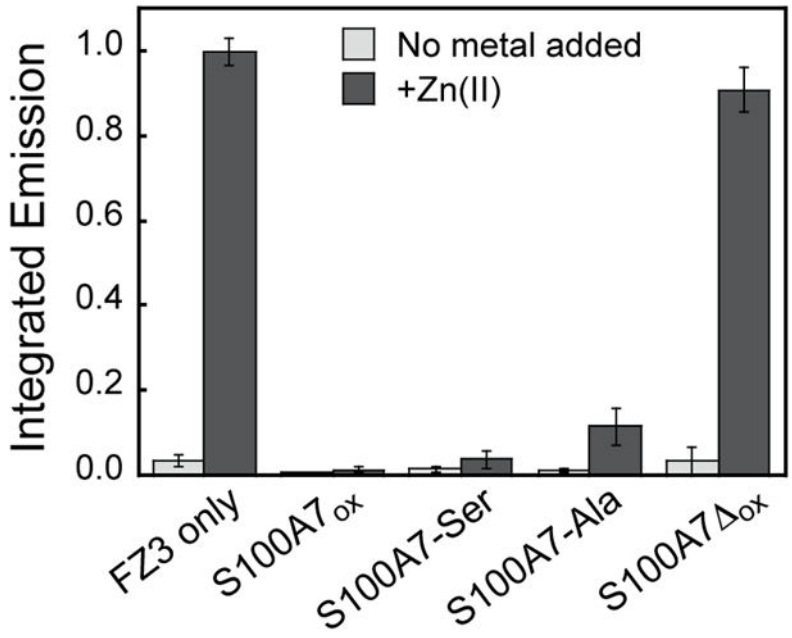

Figure 6.

S100A7 outcompetes FZ3 for Zn(II). Fluorescence response of 2 μM FZ3 to 2 μM Zn(II) in the absence and presence of 2 μM $S100A7_{ox}$, S100A7-Ser, S100A7-Ala, or $S100A7\Delta_{ox}$ at pH 7.0 (75 mM HEPES, 100 mM NaCl) and 25 °C. Integrated emission values were normalized to the maximum emission for FZ3 in the presence of 1 equiv. of Zn(II) (mean ± SDM, $n = 3$).

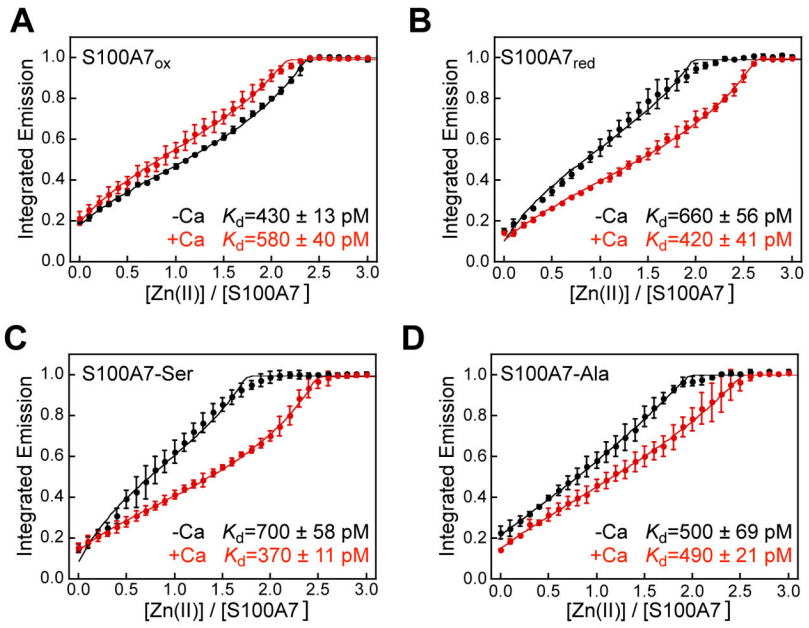

Figure 7.

Zn(II)-induced response of 2 μM ZP4 in the presence of 5 μM (A) $S100A7_{ox}$, (B) $S100A7_{red}$, (C) S100A7-Ser, and (D) S100A7-Ala at pH 7.0 (75 mM HEPES, 100 mM NaCl) at 25 °C, in the absence (black circles) and presence (red circles) of 100 equiv of Ca(II). Excitation was provided at 495 nm and the emission spectra were integrated from 505–650 nm. The integrated emission was normalized to the maximum response (mean ± SDM, n = 3). The data were fit to a two-sites binding model with $K_{d1} = K_{d2}$. The calculated apparent K_d values corresponding to the fits are listed in the bottom right of each plot.

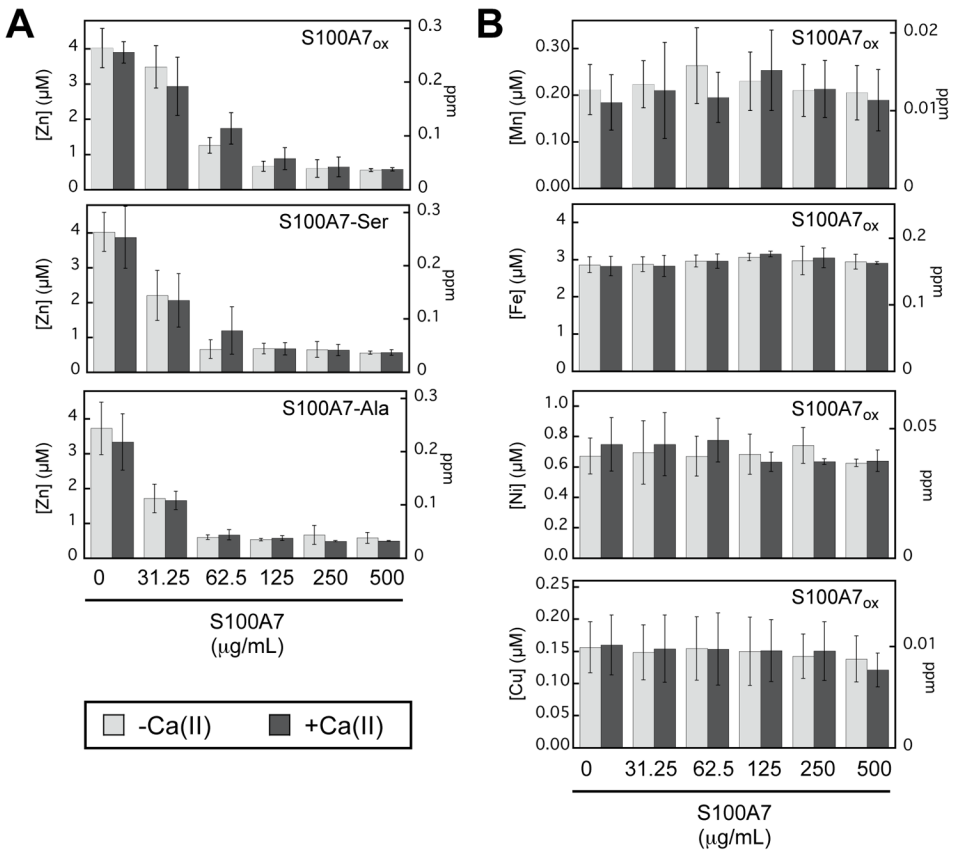

Figure 8.

S100A7 selectively depletes Zn(II) from TSB:Tris medium. Metal analysis of TSB:Tris medium treated with 0–500 μg mL^{-1} of $S100A7_{ox}$, S100A7-Ser, and S100A7-Ala. (A) Zn depletion profiles are shown for $S100A7_{ox}$, S100A7-Ser, and S100A7-Ala. (B) Mn, Fe, Ni, Cu depletion profiles are shown for $S100A7_{ox}$. The experiments were conducted in the absence (light gray bars) and presence (dark gray bars) of a 2-mM Ca(II) supplement (mean ± SDM, $n = 3$). The complete metal depletion profiles for S100A7-Ser and S100A7-Ala are presented in Figure S20.

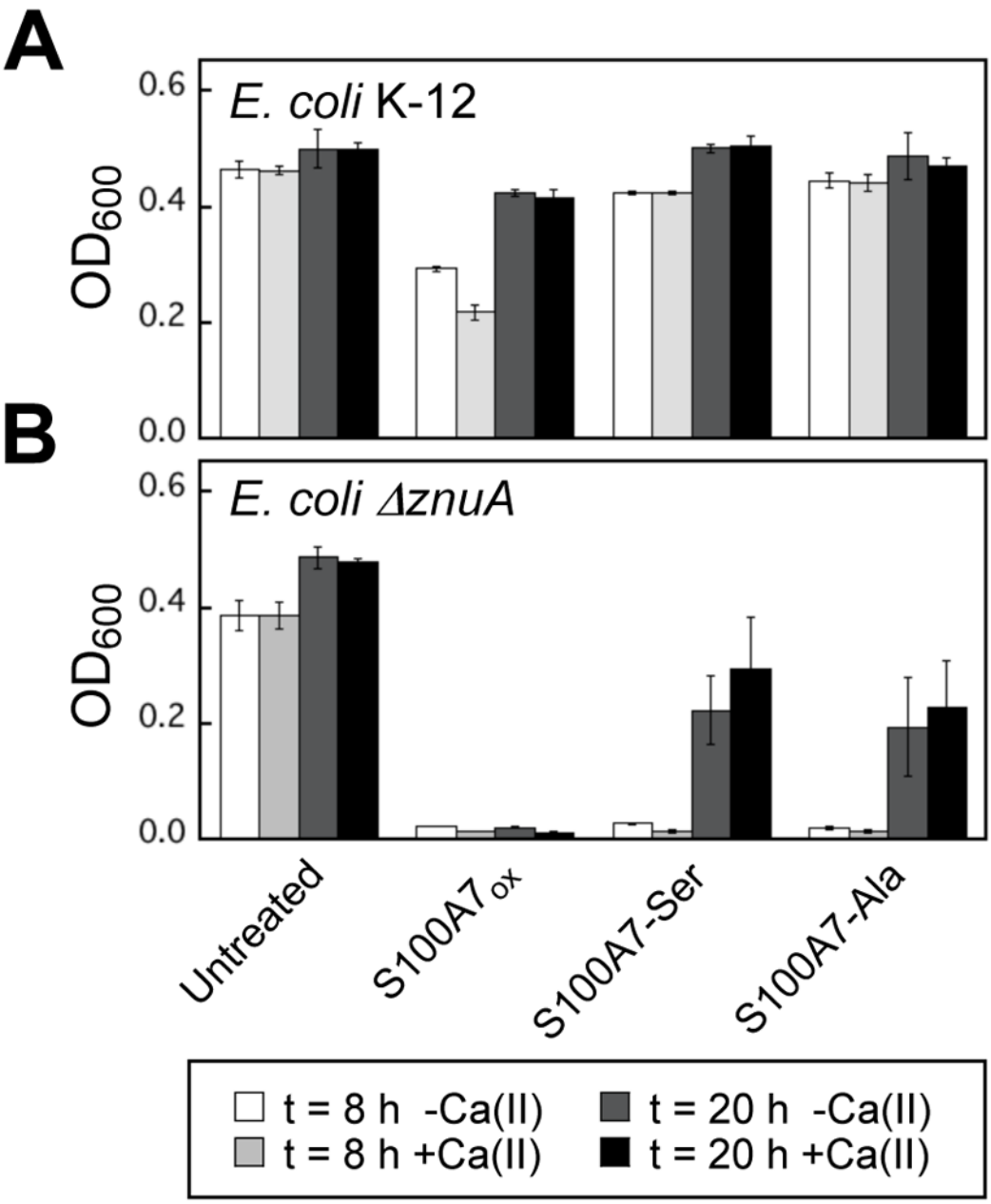

Figure 9.

Growth inhibitory activity of S100A7 against *E. coli* K-12 and the Δ*znuA* mutant in TSB:Tris medium in the absence and presence of a 2-mM Ca(II) supplement (t = 8 or 20 h, T = 37 °C). (A) *E. coli* K-12 parent strain. (B) *E. coli* Δ*znuA*. The OD_{600} values were recorded at t = 8 and 20 h (mean ± SDM, $n = 3$).

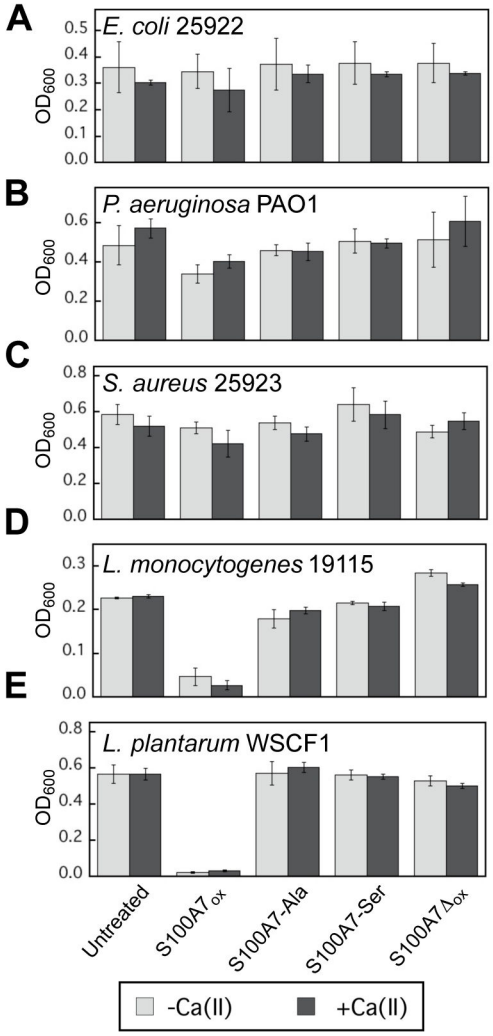

Figure 10.

Antibacterial activity of S100A7 (1000 μg/mL) against (A) *P. aeruginosa* PAO1, (B) *E. coli* ATCC 25922, (C) *S. aureus* ATCC 25923, (D) *L. monocytogenes* ATCC 19115, and (E) *L. plantarum* WSCF1. The experiments were conducted in TSB:Tris (*E. coli* and *S. aureus),* BHI:Tris (*L. monocytogenes*), and MRS:Tris (*L. plantarum*) in the absence (light gray bars) and presence (dark gray bars) of a 2-mM Ca(II) supplement (T = 30 or 37 °C, Table S21). The OD_{600} values were recorded at t = 20 h (mean ± SDM, $n = 3$).

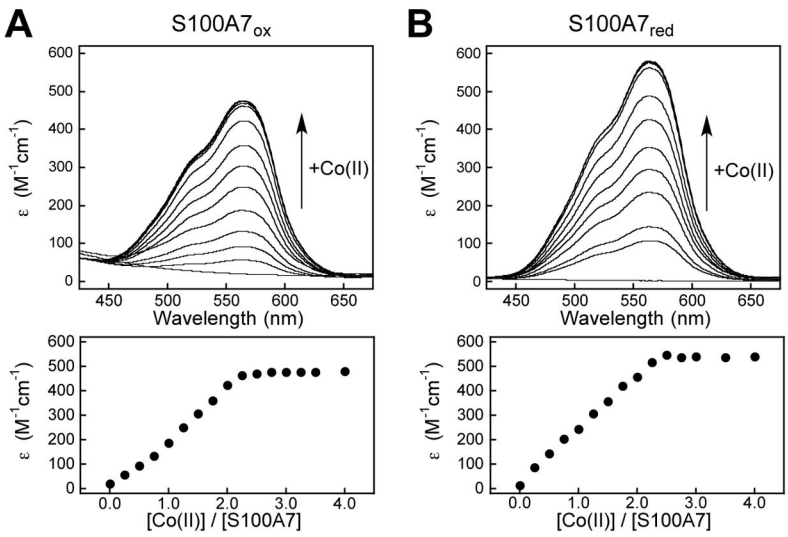

Figure 11.

Co(II)-binding titrations with $S100A7_{ox}$ and $S100A7_{red}$. Optical absorption spectra titrations (top panels) and Σ_{563} versus equivalents of Co(II) added (bottom panels) to 300 μM of $S100A7_{ox}$ (A), and $S100A7_{red}$ (B) in 75 mM HEPES, 100 mM NaCl, pH 7.0 and 25 °C. Titrations with S100A7-Ser and S100A7-Ala are presented in Figure S23. Titrations performed in the presence of 2 mM Ca(II) are presented in Figure S24.

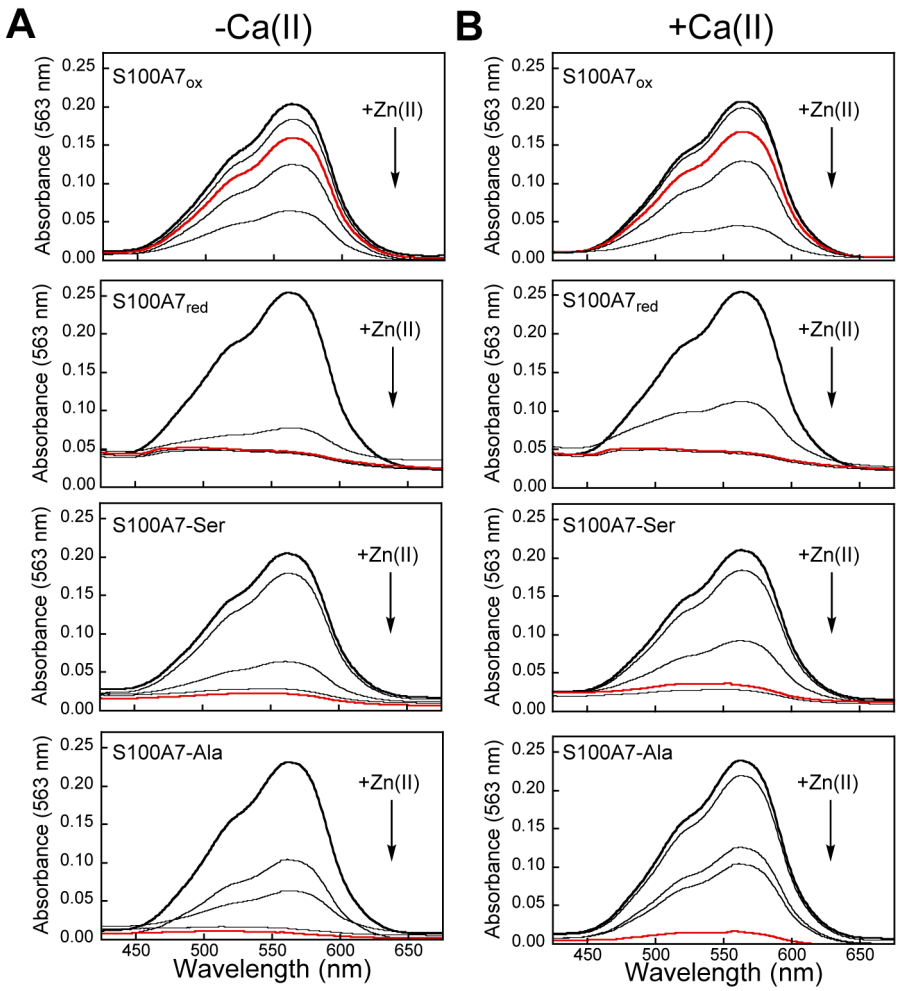

Figure 12.

Optical absorption spectra showing the substitution of Co(II) for Zn(II) at the His_3Asp sites of S100A7 in the absence (A) and presence (B) of 2 mM Ca(II). Black trace: spectrum of S100A7 (400 μM) in the presence of Co(II) (1.6 mM, 4.0 equiv) at pH 7.0 (75 mM HEPES, 100 mM NaCl, ±2 mM Ca(II)). Additional traces: after 1.6 mM Zn(II) was added to the sample. For $S100A7_{ox}$, time points were collected at 5, 60, 360, and 2400 min. For $S100A7_{red}$, S100A7-Ser and S100A7-Ala, time points were collected at 5, 20, 30 and 60 min. For all proteins, the spectrum collected at the 60 min time point is shown in red.

Table 1

Characterization of S100A7 and Variants

Protein	HPLC Retention Time (min) [a]	Free thiol [b]	Calculated Mass (Da)	Observed Mass (Da)
$S100A7_{ox}$	16.4	0.11 ± 0.03	11 454.9	11 445.4 11 324.0 (-Met1)
$S100A7_{red}$	18.4	4.16 ± 0.45	11 456.9	11 457.4 11 326.0 (-Met1)
S100A7-Ser	16.0	0.05 ± 0.01	11 424.8	11 425.5 11 294.2 (-Met1)
S100A7-Ala	16.7	0.04 ± 0.00	11 392.8	11 392.8 11 261.1 (-Met1)
$S100A7\Delta_{ox}$	21.0	0.14 ±0.04	11 212.7	11 212.9 11 082.0 (-Met1)

[a] The purified proteins are mixtures of full-length S100A7 and S100A7 lacking the Nterminal Met residue. In some chromatograms, partial separation of these two species is observed. The retention time is for the major species, which corresponds to the isoform containing the N-terminal Met residue.

[b] Free thiol content determined by using the DTDP assay (mean ± SDM, $n = 2$).